

## 2-D color code quantum computation

Austin G. Fowler

*Centre for Quantum Computer Technology, The University of Melbourne, Victoria 3010, Australia*

(Dated: September 4, 2018)

We describe in detail how to perform universal fault-tolerant quantum computation on a 2-D color code, making use of only nearest neighbor interactions. Three defects (holes) in the code are used to represent logical qubits. Triple defect logical qubits are deformed into isolated triangular sections of color code to enable transversal implementation of all single logical qubit Clifford group gates. CNOT is implemented between pairs of triple defect logical qubits via braiding.

### I. INTRODUCTION

Classical computers manipulate bits that can be exclusively 0 or 1. Quantum computers manipulate quantum bits (qubits) that can be placed in arbitrary superpositions  $\alpha|0\rangle + \beta|1\rangle$  and entangled with one another to create states such as  $(|00\rangle + |11\rangle)/\sqrt{2}$ . This additional flexibility provides both additional computing power [1–8] and additional challenges when attempting to cope with the now quantum errors in the computer [9–11]. An extremely efficient scheme for quantum error correction and fault-tolerant quantum computation is required to correct these errors without making unphysical demands on the underlying hardware and without introducing excessive time overhead and thus wasting a significant amount of the potential performance increase.

Recently, significant progress towards practical quantum error correction and fault-tolerant quantum computation has been made by making use of topological error correction [12–16]. These schemes feature a single error correcting code used for the entire computer with qubits associated with holes or “defects” deliberately introduced using measurements. Logical qubits can be initialized and measured in the  $X_L$  and  $Z_L$  bases. Logical CNOT involves braiding defects around one another. Individual logical qubits can be isolated and some transversal single logical qubit operations applied [14, 15]. All of these schemes possess a sufficiently broad range of gates to enable state distillation [17, 18] and thus achieve universality, but none possess a sufficiently broad range of gates to enable universal computation without state distillation. Indeed, it has recently been suggested that it is not possible for these types of topological schemes to avoid non-topological techniques, such as state distillation, to enable universal quantum computation [19].

State distillation is typically used to produce a better copy of one or both of the states  $|Y\rangle = (|0\rangle + i|1\rangle)/\sqrt{2}$  and  $|A\rangle = (|0\rangle + e^{i\pi/4}|1\rangle)/\sqrt{2}$  consuming either 7 or 15 imperfect copies of these states, respectively. Given reasonable assumptions about the desired logical error rate and the underlying physical error rate, three or more concatenated layers of state distillation can easily be required to produce sufficiently high fidelity states [13]. A single Toffoli gate requires 7 accurate copies of  $|A\rangle$  and up to 7 accurate copies of  $|Y\rangle$  [13, 20]. Depending on the details of the quantum algorithm being executed, the an-

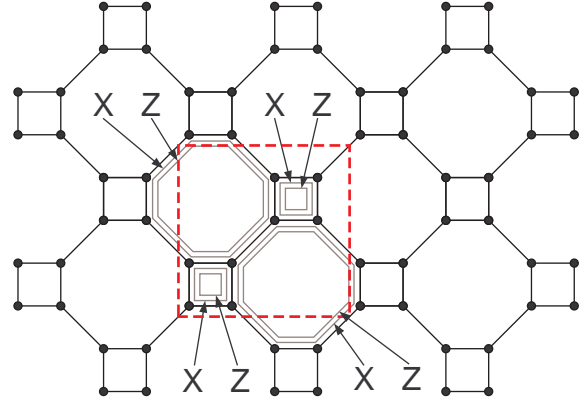


FIG. 1: The stabilizers of the error correction substrate. Dots indicate the location of qubits. The dashed box is a unit cell of the lattice containing 8 qubits and associated with 8 independent stabilizers.

cilla factory required to produce a sufficiently high rate of distilled states can easily be several orders of magnitude larger than the rest of the computer. Reducing the reliance on state distillation can thus result in a large reduction of the required number of qubits.

In this work, we combine a 2-D color code [21] with defect braiding, defect isolation and transversal rotation to enable the implementation of CNOT and the entire single qubit Clifford group of gates. This problem has also received attention in a recent work [22], however the scheme presented here is simpler. Our scheme calls for a 2-D array of qubits with local tunable interactions and a measurement time of the same order as the gate times. It features a reasonably high threshold error rate of approximately 0.1% [23]. Our scheme also supports fast long-range logical gates and relatively low qubit overhead due to both its use of efficient topological error correction and its reduced reliance on state distillation.

The discussion is organized as follows. In Section II we review a 2-D color code from [21] which forms the error correction substrate of all that follows. Logical qubit initialization and measurement are described in Section III, with each logical qubit being represented by three defects. Section IV describes defect deformation. The logical gates CNOT,  $H$ ,  $X$ ,  $Z$  and  $S$  are detailed in Section V. Section VI summarizes our results.

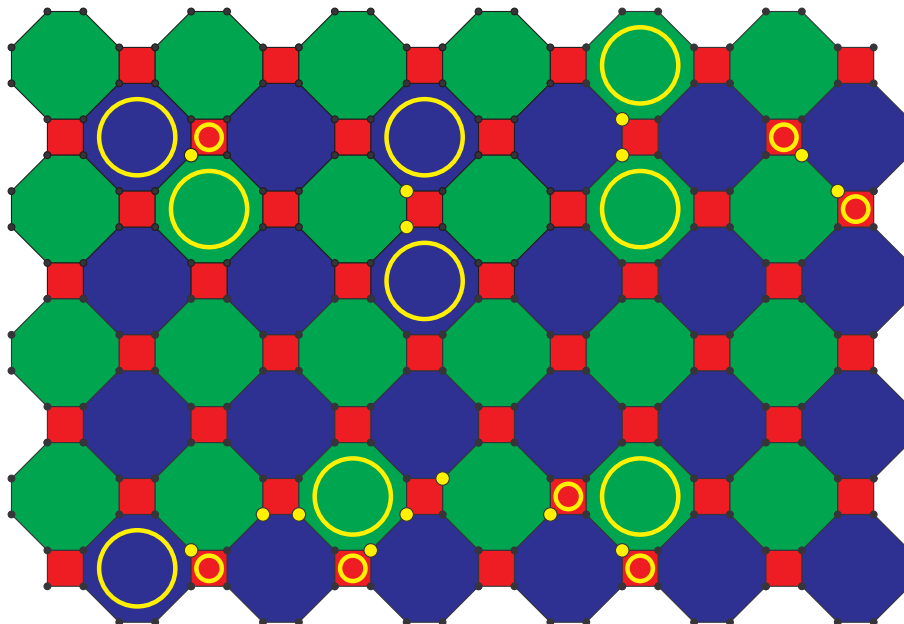


FIG. 2: Examples of errors in a color code (color online). Yellow dots indicate the locations of errors. Yellow circles indicate stabilizers of changed sign. As drawn, each chain of errors is of a single type  $X$  or  $Z$  and the neighboring stabilizers of changed sign are of type  $Z$  or  $X$ , respectively.

## II. ERROR CORRECTION SUBSTRATE

Consider Fig. 1. This shows a 2-D lattice of qubits arranged on faces with either 4 or 8 edges [21]. Each face is associated with two stabilizers [24]: the tensor product of  $X$  on every qubit around the face and similarly for  $Z$ . Note that because every face has two qubits in common with its neighboring faces, all stabilizers commute. Note also that the unit cell indicated in Fig. 1 contains 8 qubits and can be associated with 8 independent stabilizers. An infinite lattice of this form therefore contains no logical qubits. In the absence of errors, the lattice of qubits may be assumed to be in the simultaneous  $+1$  eigenstate of each stabilizer.

Fig. 2 contains examples of the effects of errors. Note that one of the three colors red, blue and green has been assigned to each of the faces such that no two adjacent faces have the same color. This will simplify the discussion of the various types of errors and the later discussion of logical operators. Every qubit is on three faces. If a qubit suffers an  $X/Z$  error, the  $Z/X$  stabilizers of these three faces become negative if no other error of the same type occurs on these three faces. A second error of the same type adjacent to the first error results in just two faces of the same color having negative stabilizers. Such chains of errors are said to have the same color as the faces they connect. A chain of each color can meet at a single qubit without changing the sign of any stabilizers. Arbitrarily complex error trees can occur with multiple intersections.

Additional syndrome qubits are required to determine

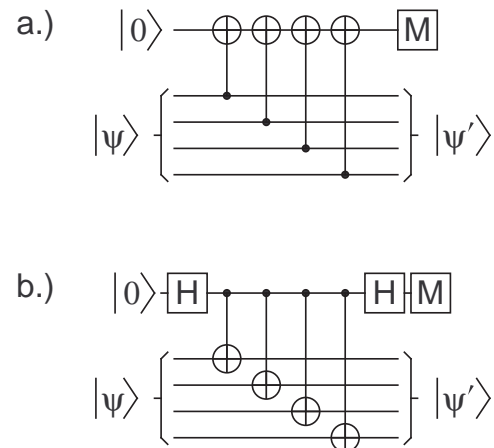


FIG. 3: Circuit showing how an additional syndrome qubit (top line of each figure) is used to measure red face a.)  $Z$  stabilizers, b.)  $X$  stabilizers.

the sign of the face stabilizers. For red faces we choose to use just one additional syndrome qubit and the simple circuits shown in Fig. 3 to determine the sign of their associated  $X$  and  $Z$  stabilizers. Note that errors occurring during these circuits can propagate to the data qubits with a single syndrome qubit error propagating to multiple data qubits. For red faces, the potential number of effected data qubits is sufficiently low that we choose to leave the detection and correction of these errors to later rounds of syndrome extraction.

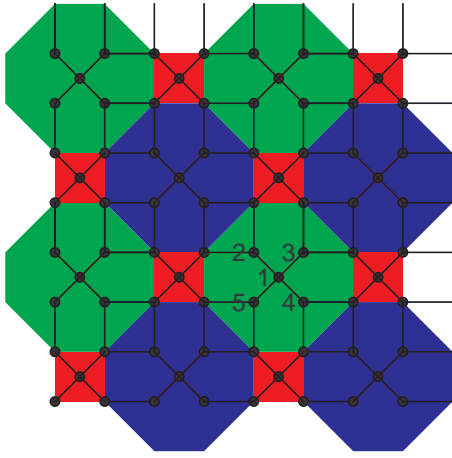


FIG. 4: Underlying lattice of physical qubits. Dots represent qubits, lines represent tunable interactions between qubits. The numbered qubits are used in Figs. 6–7.

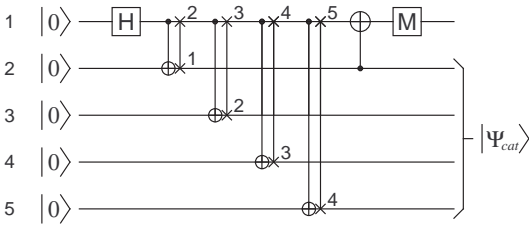


FIG. 5: Preparation of a 4-qubit cat state using the 5 qubits indicated in Fig. 4. The states initially stored in qubits 1–4 are manipulated to form a cat state stored on qubits 2–5. The state stored in qubit 5 is used to check the cat state and is read out using qubit 1.

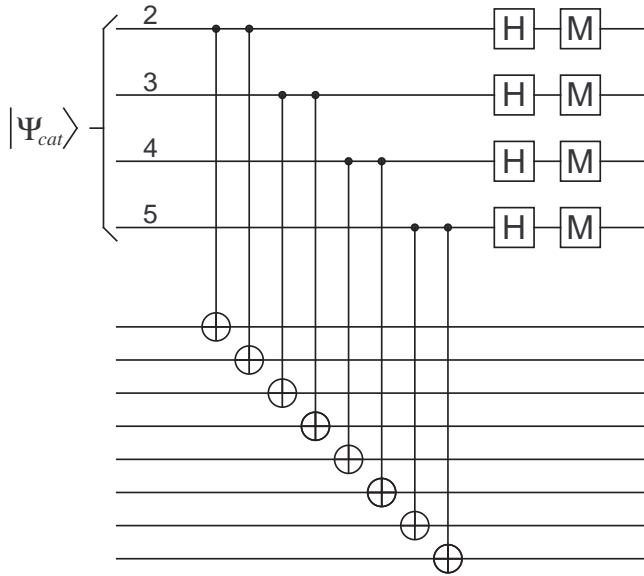


FIG. 6: Circuit used to determine the eigenvalue of the 8 qubit  $X$  stabilizer associated with a green or blue face.

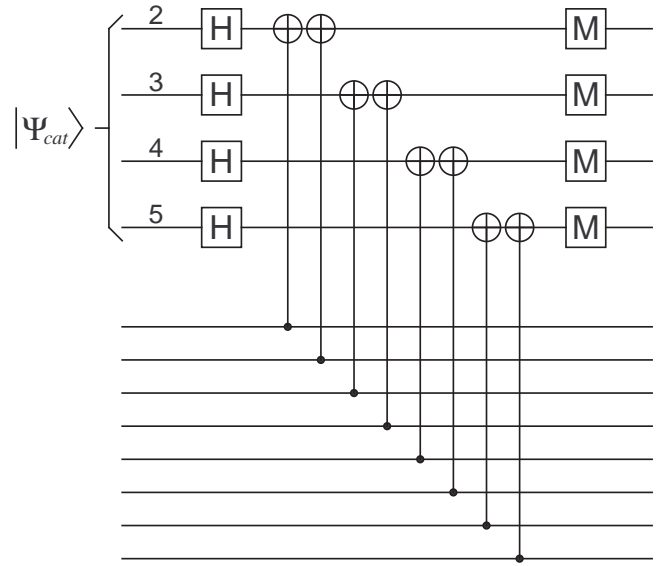


FIG. 7: Circuit used to determine the eigenvalue of the 8 qubit  $Z$  stabilizer associated with a green or blue face.

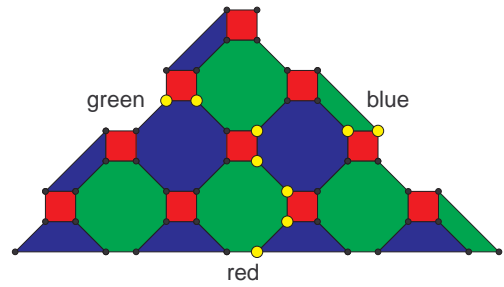


FIG. 8: Examples of the three colors of boundaries and error chains of each color starting at each boundary and meeting a single qubit.

Green and blue faces, with 8 data qubits, could simply use the 8 qubit analogues of Fig. 3 and live with the fact that up to 4 data qubits could be effected by an error on the single syndrome qubit. We choose not to do this. Instead, 5 syndrome qubits are devoted to each green and blue face as shown in Fig. 4. Initially, the circuit of Fig. 5 is repeatedly executed until the central syndrome qubit is measured in state  $|0\rangle$  indicating successful preparation of a 4-qubit cat state provided no more than one error occurred during the execution of the circuit. The circuits of Fig. 6 and Fig. 7 are then executed for  $X$  and  $Z$  syndrome extraction respectively with each qubit of the cat state interacting with its two non-syndrome nearest neighbors.

In addition to reducing the number of data qubits that can be corrupted after a single error during syndrome extraction, a significant benefit of using 5 syndrome qubits on green and blue faces is avoiding the need to have a single syndrome qubit coupled to 8 data qubits, greatly

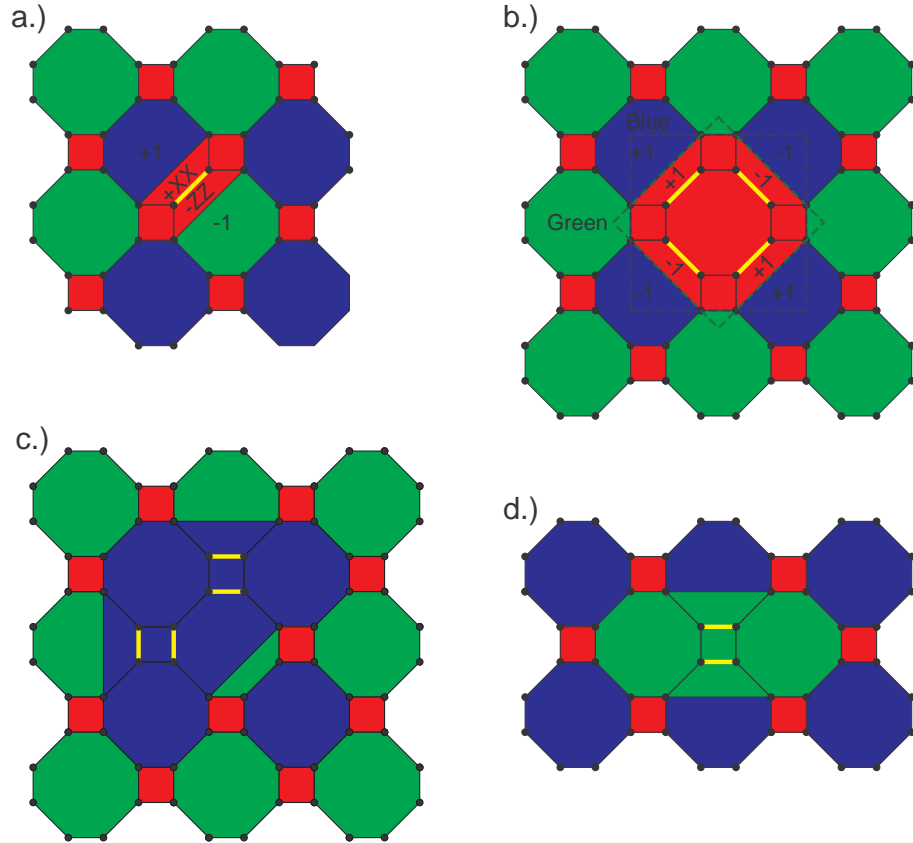


FIG. 9: a.) Red defect created by measuring  $XX$  and  $ZZ$  on the qubits indicated by a yellow line (color online). The signs of these measurements determine the signs of the stabilizers of the neighboring faces of reduced size. b.) Red defect created by measuring a complete face. Equivalent blue and green boundary stabilizers with positive sign independent of the measurement results assuming no errors. These boundary stabilizers are always positive as they are equal to the product of the five complete face stabilizers contained within the effect. c.) Blue defect. d.) Green defect.

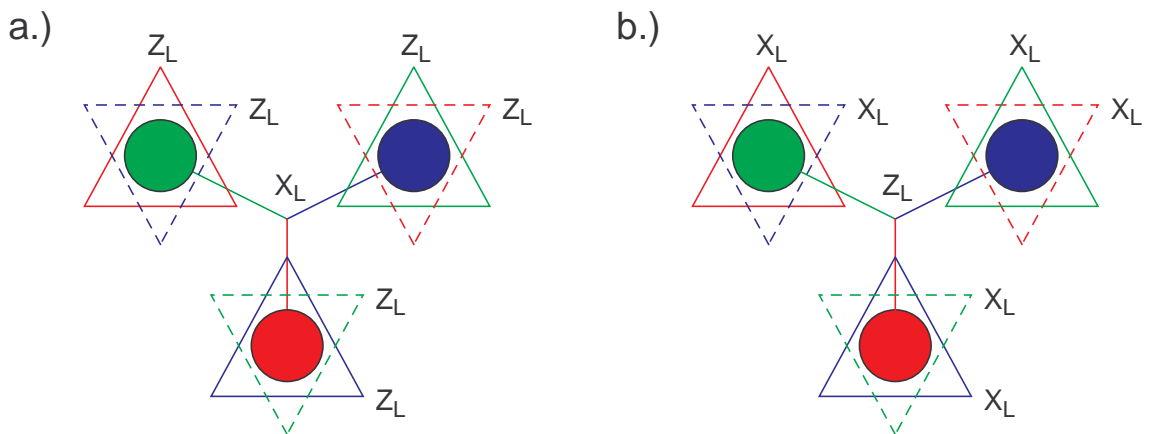


FIG. 10: A defect of each color forming a.) a primal qubit, b.) a dual qubit. Note that the six primal  $Z_L$  and dual  $X_L$  operators are equivalent.

simplifying the underlying lattice of qubits and network of connections. Note that in Fig. 4 no qubit is connected to more than 4 other qubits with most connected to just 3 other qubits. Note also that the concepts of color and the different face sizes arise only from how the underlying hardware is used, not from any aspect of its physical construction.

The lattices we will discuss in this work will both have and make extensive use of boundaries. Fig. 8 shows examples of the three different colors of boundaries. At this point in the discussion, the only property of a boundary of a given color that is of interest is the fact that an error chain of the same color can connect to it without changing the sign of any stabilizers. An example of an error chain of each color starting at each boundary and meeting at a single qubit is shown. The details of how error correction might be performed and a calculation of the threshold error rate can be found in [23].

### III. LOGICAL QUBIT INITIALIZATION AND MEASUREMENT

In Section II we discussed an infinite lattice of qubits and error correction circuits, however the lattice contained no logical qubits. Logical qubits can be introduced by ceasing to enforce stabilizers and thereby introducing degrees of freedom into the lattice. We call a connected region of a single color of faces whose stabilizers we no longer enforce a defect. Examples of red, green and blue defects are shown in Fig. 9. Note that by connected we mean faces connected by an  $XX$  and a  $ZZ$  measurement. The effect of these measurements is to create a single large face of the same color as the constituent faces. Initially, provided the defect is constructed from the measurement of complete faces, it is in the  $+1$  eigenstate of its associated bounding  $X$  and  $Z$  stabilizers. We will henceforth always use defects constructed from the measurement of complete faces. Note that the bounding stabilizers can be regarded as rings of either of the two colors the defect isn't.

Before a defect can be used as part of a logical qubit, some of its neighboring stabilizers must be corrected. Stabilizers that have had their sides reduced by  $XX$  and  $ZZ$  measurements will have a sign dependent on the results of these measurements. Note that such reduced size stabilizers of negative sign always occur in pairs. They can therefore also be connected and corrected in pairs using appropriate chains of operators.

Note that direct  $XX$  and  $ZZ$  measurements are actually not necessary to create a large defect. It is equivalent and simpler to just measure the stabilizers of reduced size. The qubits inside the defect can be ignored. These inner qubits only become important again if the size of the defect is reduced.

Many types of logical qubits are possible. We will be interested in logical qubits consisting of three defects, one of each color. Note that chains of operators of the same

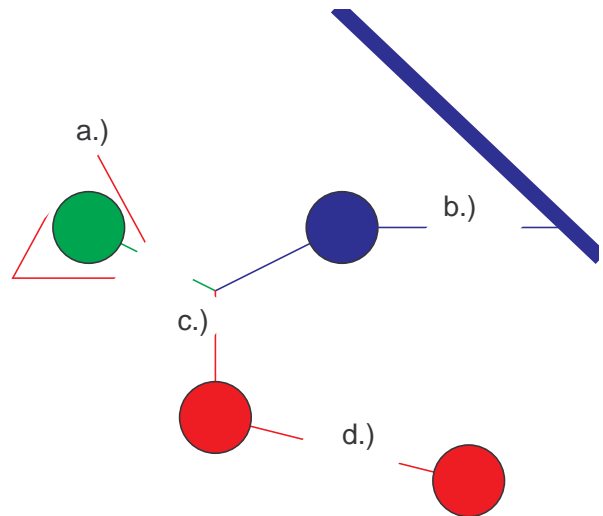


FIG. 11: Examples of error chains likely to lead to logical errors. a.) Half encircling a defect. b.) Half connecting a defect to a boundary of the same color. c.) Half connecting the three defects. d.) Half connecting a defect to another of the same color.

color commute regardless of whether they consist of  $X$  or  $Z$  operators as they always have an even number of qubits in common. Fig. 10 shows examples of the two types of triple defect logical qubits we will use. We call logical qubits with triangular  $X_L$  operators “primal” and those with triangular  $Z_L$  operators “dual”. Primal qubits will store the data in our computer whereas dual qubits will facilitate multiple qubit gates. Note that the six types of primal  $Z_L$  operators are equivalent in the sense that they all commute with one another and all anticommute with primal  $X_L$ . When performing a logical phase-flip, it does not matter which primal  $Z_L$  operator is used. Dual  $X_L$  operators are also all equivalent.

Primal qubits are naturally initialized to the  $+1$  eigenstate of  $Z_L$ , namely  $|0_L\rangle$ . Similarly, dual qubits are naturally initialized to  $|+_L\rangle$ . Note that since primal and dual qubits are structurally identical, when we create a logical qubit we actually create both a primal and a dual qubit. Furthermore, we do nothing to distinguish these two types of qubits. As we shall see, computation proceeds with both types of qubit present and we simply ignore one type and focus on the computation occurring in the qubit type of interest.

Measurement of a logical qubit can be performed transversely by measuring a region of qubits encompassing the three defects in either the  $X$  or  $Z$  basis. Measurement results are error corrected using the standard algorithm with syndromes calculated from the parity of measurement results around each face. After error correction, provided no logical errors have occurred, all rings of measurements around each defect will have the same parity and similarly all three-way chains of measurements connecting all three defects will have the same parity. These

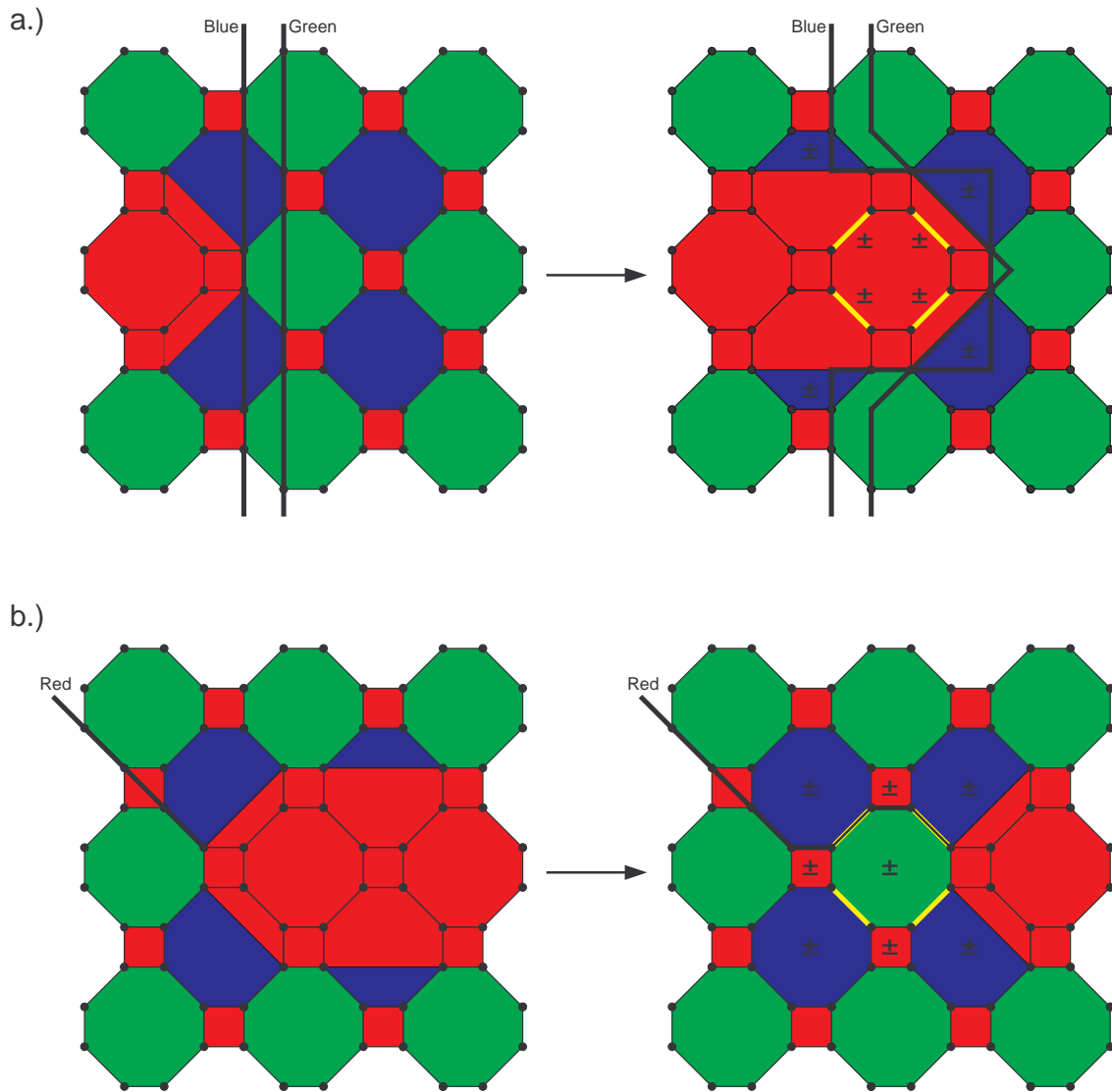


FIG. 12: a.) Procedure for expanding a red defect. It is conceptually simpler to imagine that the operators  $XX$  and  $ZZ$  are measured directly on the qubits on the yellow lines (color online), but in practice these qubits can be ignored and only the stabilizers of the indicated partial faces measured. b.) Procedure for contracting a red defect. The full stabilizers of the indicated faces are measured once more. The signs of these face stabilizers are then corrected using the regular error correction procedure.

parities are the logical measurement results. Note that when performing the transversal  $X/Z$  measurements we perform both a primal and a dual  $X_L/Z_L$  measurement. The unnecessary logical measurement result is simply ignored.

Primal/dual qubits can also be initialized to  $|+_L\rangle/|0_L\rangle$  by first initializing a region of qubits to  $|+\rangle/|0\rangle$  and then creating defects by measuring appropriate  $Z/X$  stabilizers. These stabilizers will have random sign initially, and must be corrected before the logical qubit is used.

A number of different types of logical errors are possible. Fig. 11 contains a few examples. If an error chain half encircles a defect, it cannot be reliably corrected as

given only endpoint information is not possible to know which half of the defect is encircled and thus which half of the defect to apply corrective operations to. If the wrong half is chosen, we form a logical operation instead of correcting the error. For primal/dual qubits, half rings of  $Z/X$  errors are dangerous. Similarly, if a collection of different color error chains half constructs a three-way connection, the error correction procedure cannot in general determine which half has been constructed and correct it. For primal/dual qubits, half connections of  $X/Z$  errors are dangerous. Furthermore, individual defects of a given color can be half connected to other defects of the same color by error chains or half connected to boundaries of

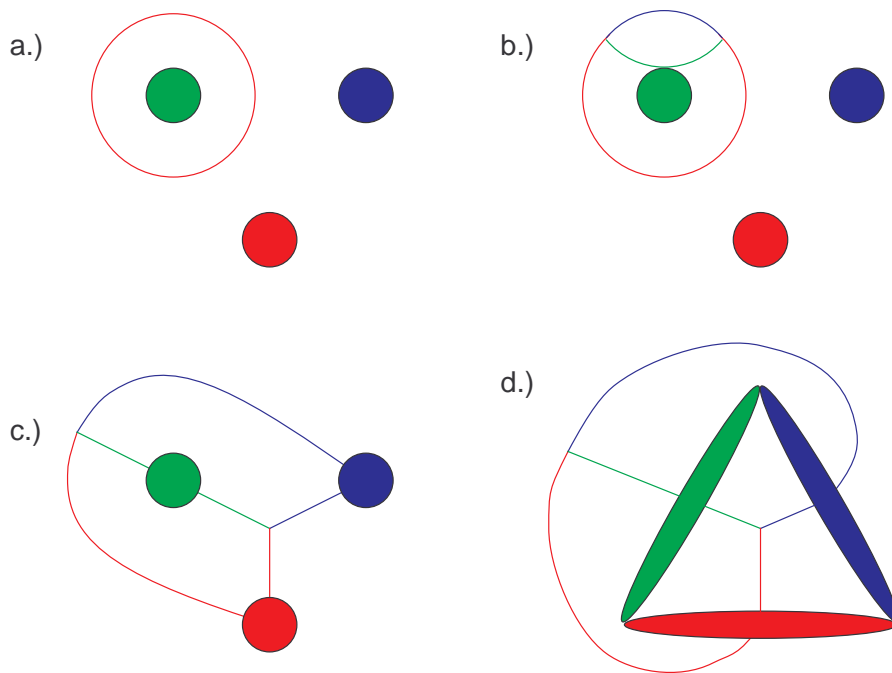


FIG. 13: Step-by-step deformation of a ring operator into a pair of tree operators via deformation of the associated defects to create an isolated region of lattice.

the same color. Both situations correspond to errors that cannot be reliably corrected. Given the rich error structure of color codes, an unlimited number of additional types of logical errors are possible, though suppressed if boundaries and defects are kept well separated. Note that the strength of  $X/Z$  error correction can be independently set by adjusting the circumference and separation of defects.

#### IV. DEFECT DEFORMATION

We have discussed error correction and the creation and measurement of logical qubits. We now turn our attention to the techniques required to perform computation. Defect expansion and contraction can be used to adjust the size of a defect and thus the local error correction strength. By combining expansion and contraction, defects can be moved and braided around one another, realizing multiple qubit gates as we shall see in Section V. Expanding all three defects comprising a logical qubit until they touch and creating an enclosed triangular region isolates the logical qubit from the rest of the lattice, enabling transversal gates to be applied.

Consider Fig. 12a. This shows the procedure for expanding a red defect and the effect of doing so on both a green and blue stabilizer. Fig. 12b shows the effect of contracting a defect on a red stabilizer attached to the defect. Note that even in the absence of errors, corrective operations must be applied when moving the defect to en-

sure that the signs of all stabilizers remain unchanged at the end of the procedure. The procedures for expanding and contracting green and blue defects are analogous.

Fig. 13 shows the effect of isolating a triangular region of the lattice, the detailed structure of which can be found in Fig. 8, by simultaneously expanding all three defects comprising a logical qubit. Stabilizers encircling a defect are converted into pairs of three-way stabilizers. Section V makes use of such isolated regions. Note that the isolation is reversible by simply contracting the defects once more.

#### V. LOGICAL GATES

In this section, we describe the logical gates CNOT,  $H$ ,  $X$ ,  $Z$  and  $S$ . By far the simplest logical gates are  $X_L$  and  $Z_L$ , which can be implemented with simple rings and three-way trees of single-qubit operators. We shall not discuss these further. The remaining logical gates require individual discussion.

Logical Hadamard,  $H_L$ , shall be applied transversely to an isolated triangular logical qubit, however some care is required. Given a primal/dual qubit, during the isolation process  $Z_L/X_L$  is split into two three-way trees. The tree external to the isolated region must be removed before transversal gates can be applied. This can be achieved by measuring a region of qubits around the isolated region in the  $Z/X$  basis. Note that all external operator trees must have the same parity in the absence of errors and

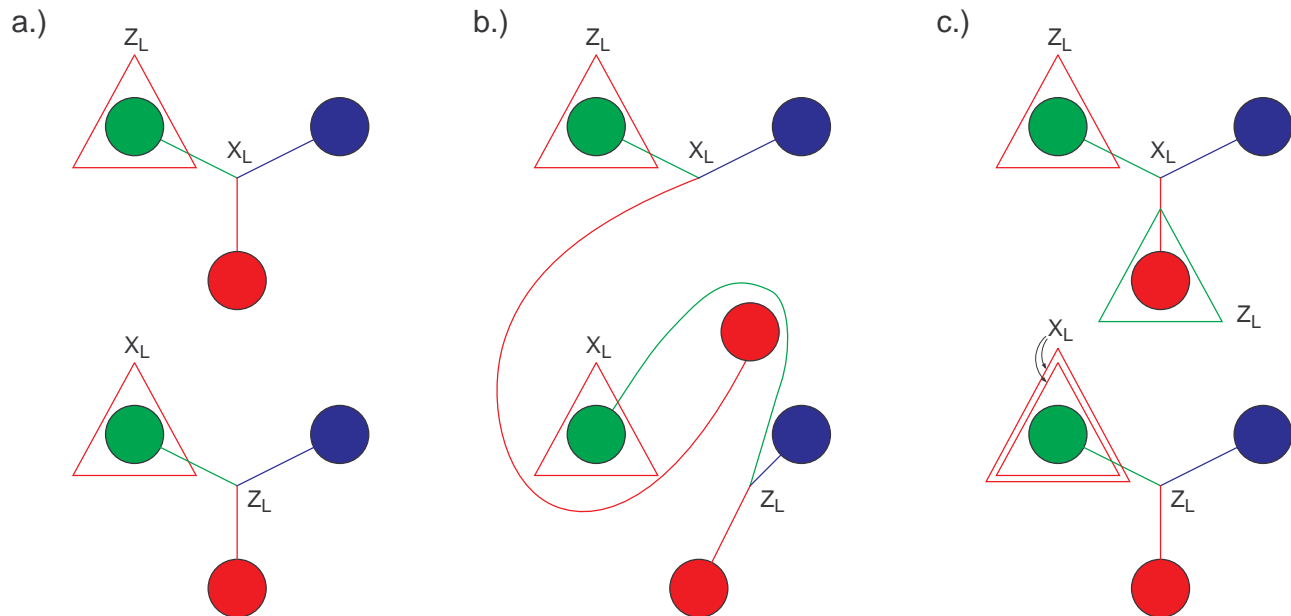


FIG. 14: Logical CNOT via braiding with a primal qubit (top) as control and dual qubit (bottom) as target. The appropriate mappings of logical stabilizers  $XI \mapsto XX$ ,  $IX \mapsto IX$ ,  $ZI \mapsto ZI$  and  $IZ \mapsto ZZ$  can be seen by tracing the deformation of one logical stabilizer at a time.

that the standard error correction procedure can be used to ensure that the parity is determined fault-tolerantly. Note that this does not constitute logical measurement of  $Z_L/X_L$  as the isolated region is not measured and the parity of internal three-way trees must also be known to effect logical measurement. Measuring the parity  $s$  of external trees does, however, introduce a byproduct operator  $X_L^s/Z_L^s$ . With the external trees pruned, logical Hadamard can then be applied transversely. The appropriate external face stabilizers must be measured and corrected before the logical qubit is converted back to three isolated defects. The conversion back can also introduce a byproduct operator.

Logical  $S$  requires a different type of care. In this case, the external trees do not need to be pruned, however we need to ensure that the correct number of qubits have been enclosed. In the original color code work, triangular logical qubits with  $3 \bmod 4$  total physical qubits and either 4 or 8 qubits per face were used [21]. For convenience, we require there to be  $1 \bmod 4$  enclosed qubits. Using enclosed regions of the form shown in Fig. 8, this can be achieved by having an even number of rows of red faces. When single-qubit  $S$  is applied transversely, the condition of having either 4 or 8 qubits per face ensures that every state comprising  $|0_L\rangle$  and every state comprising  $|1_L\rangle$  acquires the same phase. Having  $1 \bmod 4$  qubits in total ensures that  $|0_L\rangle \mapsto |0_L\rangle$  and  $|1_L\rangle \mapsto i|1_L\rangle$ . Transversal  $S$  thus implements  $S_L$ .

With an odd number of enclosed qubits and every three-way chain containing an odd number of operators, we can also implement  $X_L$  and  $Z_L$  transversely. While

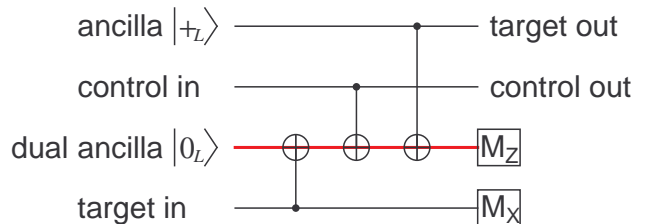


FIG. 15: Circuit constructed from available components implementing primal-primal logical qubit CNOT.

this would not be done under normal circumstances, as it is easier to simply apply ring or tree operators to non-isolated logical qubits, if the logical qubit has already been isolated, the ability to apply transversal  $X_L$  and  $Z_L$  enables us to avoid further modification of the shape of the logical qubit.

Logical CNOT is carried out in a similar manner to the schemes of [13, 15]. A primal qubit can be used to control a CNOT gate with a dual qubit as target as shown in Fig. 14. Note that all of the CNOT stabilizer mappings  $XI \mapsto XX$ ,  $IX \mapsto IX$ ,  $ZI \mapsto ZI$  and  $IZ \mapsto ZZ$  are faithfully realized. We can then use the circuit shown in Fig. 15 to simulate CNOT between two primal qubits.



## VI. CONCLUSION

We have described how to perform universal fault-tolerant quantum computation with reduced reliance on state distillation on a specific 2-D color code. This scheme has a relatively high threshold error rate of 0.1%, relatively low qubit overhead, fast long-range logical gates and makes few demands on the underlying hardware. Our scheme calls for a measurement time of the same order as the gate times, local single qubit unitaries

and a 2-D nearest neighbor tunably coupled lattice of qubits, with each qubit coupled to either 3 or 4 neighbors and with no couplings crossing. This lattice is shown in Fig. 4. Ideally, it should be possible to simultaneously measure an arbitrary subset of qubits in the lattice, although if measurement hardware cannot be located near every qubit, it would be sufficient to be able to measure a fraction of the qubits that is independent of the lattice size.

- 
- [1] P. W. Shor, in *Proc. 35th Annual Symposium on Foundations of Computer Science* (1994), pp. 124–134, quant-ph/9508027.
  - [2] L. K. Grover, in *Proc. Twenty-Eighth Annual ACM Symposium on the Theory of Computing* (1996), pp. 212–219, quant-ph/9605043.
  - [3] V. Subramaniam and P. Ramadevi, quant-ph/0210095 (2002).
  - [4] D. Cheung, D. Maslov, J. Mathew, and D. K. Pradhan, *Quant. Info. Comp.* **9**, 610 (2009), arXiv:0710.1093.
  - [5] A. W. Harrow, A. Hassidim, and S. Lloyd, *Phys. Rev. Lett.* **103**, 150502 (2009), arXiv:0811.3171.
  - [6] S. Lloyd, *Science* **273**, 1073 (1996).
  - [7] N. Wiebe, D. W. Berry, P. Hoyer, and B. C. Sanders, arXiv:1011.3489 (2010).
  - [8] J. Smith and M. Mosca, arXiv:1001.0767 (2010).
  - [9] P. W. Shor, *Phys. Rev. A* **52**, R2493 (1995).
  - [10] A. R. Calderbank and P. W. Shor, *Phys. Rev. A* **54**, 1098 (1996), quant-ph/9512032.
  - [11] A. M. Steane, *Proc. R. Soc. Lond. A* **452**, 2551 (1996), quant-ph/9601029.
  - [12] R. Raussendorf and J. Harrington, *Phys. Rev. Lett.* **98**, 190504 (2007), quant-ph/0610082.
  - [13] R. Raussendorf, J. Harrington, and K. Goyal, *New J. Phys.* **9**, 199 (2007), quant-ph/0703143.
  - [14] H. Bombin and M. A. Martin-Delgado, *J. Phys. A: Math. Theor.* **42**, 095302 (2009), arXiv:0704.2540.
  - [15] A. G. Fowler, A. M. Stephens, and P. Groszkowski, *Phys. Rev. A* **80**, 052312 (2009), arXiv:0803.0272.
  - [16] D. S. Wang, A. G. Fowler, and L. C. L. Hollenberg, arXiv:1009.3686 (2010).
  - [17] S. Bravyi and A. Kitaev, *Phys. Rev. A* **71**, 022316 (2005), quant-ph/0403025.
  - [18] B. W. Reichardt, *Quant. Info. Proc.* **4**, 251 (2005), quant-ph/0411036.
  - [19] P. Sarvepalli and R. Raussendorf, *Phys. Rev. A* **82**, 022304 (2010), arXiv:0911.1571.
  - [20] M. A. Nielsen and I. L. Chuang, *Quantum Computation and Quantum Information* (Cambridge University Press, Cambridge, 2000).
  - [21] H. Bombin and M. A. Martin-Delgado, *Phys. Rev. Lett.* **97**, 180501 (2006), quant-ph/0605138.
  - [22] H. Bombin, arXiv:1006.5260 (2010).
  - [23] D. S. Wang, A. G. Fowler, C. D. Hill, and L. C. L. Hollenberg, *Quant. Info. Comp.* **10**, 780 (2010), arXiv:0907.1708.
  - [24] D. Gottesman, Ph.D. thesis, Caltech (1997), quant-ph/9705052.